# Modeling Eddy Current Losses in HTS Tapes Using Multiharmonic Method

J. Ruuskanen, M. Lyly, A. Halbach, T. Tarhasaari, V. Lahtinen, T. Salmi, and P. Rasilo, *Member, IEEE*

***Abstract*—Due to the highly nonlinear electrical resistivity of high temperature superconducting (HTS) materials, computing the steady-state eddy current losses in HTS tapes, under time-periodic alternating current excitation, can be time consuming when using a time-transient method (TTM). The computation can require several periods to be solved with a small time-step. One alternative to the TTM is the multiharmonic method (MHM) where the Fourier basis is used to approximate the Maxwell fields in time. The method allows obtaining the steady-state solution to the problem with one resolution of the nonlinear problem. In this work, using the finite element method with the $H - \varphi$ formulation, the capabilities of the MHM in the computational eddy current loss modeling of HTS tapes are scrutinized and compared against the TTM.**

***Index Terms*—AC losses, finite element methods, superconducting tapes.**

## I. Introduction

REBCO based high temperature superconductors (HTS) are gaining interest in increasing amount due to their high operation temperature compared to their lower temperature superconductor counterparts [1]. The ability to operate at higher temperature can result in significant cost and energy savings when developing, testing and operating superconducting applications especially in the larger scale.

For the large scale applications such as particle accelerator magnets [2] or energy applications [3], [4], the individual REBCO tapes are typically assembled into a cable consisting of multiple tapes. There are several different REBCO tape based cable types for different applications such as Roebel cable [5], CORC [6] or STAR wire [7]. The tape configuration in the cables reduces the induced losses due to a changing magnetic field.

When designing such cables from the electromagnetic point of view, numerical computational methods are essential. One of the most popular methods is the finite element method (FEM) used to solve Maxwell's magnetoquasistatic equations coupled with the material equations. Typically, the main interest from the electromagnetic point of view are the Joule losses which act as a direct heat source for the superconducting system. The heating decreases the efficiency of the application and in the worst case can lead to quenching of the superconducting state.

Due to the highly nonlinear electrical resistivity of the HTS materials, computing eddy current losses in HTS tape based applications can be time consuming and convergence problems can occur. In the typical approach, the time-dependent models are solved with a time-transient method (TTM), where the time-evolution of the fields to be solved are computed one time-step at a time. Obtaining the steady-state solution to the problem with highly nonlinear materials with TTM can require several periods of excitation to be solved with a small time-step.

One alternative to the TTM is the multiharmonic method [8], [9] (MHM), or the harmonic balance method, where the Fourier basis is used to approximate the solution in time. The method allows obtaining the steady-state solution with one resolution of the nonlinear problem. The potential drawback in using the MHM is that when approximating behavior not natural for the chosen global basis in time, the number of required harmonics can increase beyond feasible limit in terms of computational burden.

In order to gain understanding on the capabilities of the MHM method applied to HTS modeling, the $H - \varphi$ formulation [10] was implemented to model AC losses in a HTS tape using FEM. The modeling domain and the details about the modeling task are presented in Section II. In Section III, the results comparing the predictions given by the MHM and the TTM are shown.

## II. Methodology

### A. Finite Element Model

In this paper, the MHM is compared against the TTM in a 2-D modeling domain consisting of an HTS tape cross-section surrounded by an air domain having a radius of 8 cm. The 4 mm wide and 95 $\mu$m thick tape consists of several layers of different materials as depicted in Fig. 1. At the top and bottom there are 20 $\mu$m thick copper (Cu) layers. The steel alloy (Hast) has a thickness of 50 $\mu$m and each of the two silver (Ag) layer have the thicknesses of 2 $\mu$m. The superconducting layer (HTS) is 1 $\mu$m thick [11]. The mesh of the air domain surrounding the tape is also depicted in the figure. Note that all the material layers in the tape are meshed and modeled individually, hence e.g. homogenisation techniques were not used.

Manuscript received 7 November 2022; revised 17 January 2023; accepted 1 February 2023. Date of publication 6 February 2023; date of current version 15 March 2023. This work was supported in part by the Academy of Finland under Grant 324887 and in part by the Ulla Tuominen Foundation. *(Corresponding author: J. Ruuskanen.)*

J. Ruuskanen, T. Tarhasaari, T. Salmi, and P. Rasilo are with the Electrical Engineering Unit, Tampere University, 33720 Tampere, Pirkanmaa, Finland (e-mail: janne.ruuskanen@tuni.fi; timo.tarhasaari@tuni.fi; tiina.salmi@tuni.fi; paavo.rasilo@tuni.fi).

M. Lyly is with the Electrical Engineering Unit, Tampere University, 33720 Tampere, Pirkanmaa, Finland, and also with Quanscient Oy, 33100 Tampere, Finland (e-mail: mika.lyly@tuni.fi).

A. Halbach and V. Lahtinen are with Quanscient Oy, 33100 Tampere, Finland (e-mail: alexandre.halbach@quanscient.com; valtteri.lahtinen@quanscient.com).

Color versions of one or more figures in this article are available at https://doi.org/10.1109/TASC.2023.3242619.

Digital Object Identifier 10.1109/TASC.2023.3242619

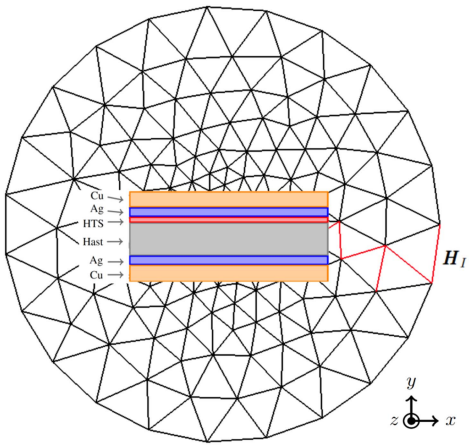


Fig. 1. Depiction of the modeling domain with the HTS tape cross-section consisting of the different material layers. Also the cohomology source field $\boldsymbol{H}_I$ is shown.

The $H-\varphi$ formulation is used where we solve for Faraday's law

$$\operatorname{curl} \boldsymbol{E} + \partial_t \boldsymbol{B} = 0, \tag{1}$$

where the field quantities $\boldsymbol{E}$ and $\boldsymbol{B}$ are the electric field strength and the magnetic flux density. To note, in the 2-D problem scrutinized in this work, the magnetic field is in the plane and consequently, the electric field strength $\boldsymbol{E}$ and the electric current density $\boldsymbol{J}$ have only the out-of-plane component. Ampère's law relates the electric current density $\boldsymbol{J}$ to the magnetic field strength $\boldsymbol{H}$ as $\boldsymbol{J} = \operatorname{curl} \boldsymbol{H}$. The constitutive relations used in the formulation are

$$\boldsymbol{E} = \rho \boldsymbol{J} \quad \text{and} \quad \boldsymbol{B} = \mu \boldsymbol{H}, \tag{2}$$

where $\rho$ is the electrical resistivity and $\mu$ the permeability. The models for these materials are detailed in Section II-B.

In this formulation, the unknown field quantity $\boldsymbol{H}$ is decomposed as follows. In the conducting domain, $\boldsymbol{H} = \boldsymbol{H}_{\mathrm{c}} + \operatorname{grad} \varphi + \boldsymbol{H}_I$ and in the nonconducting domain $\boldsymbol{H} = \operatorname{grad} \varphi + \boldsymbol{H}_I$, where $\varphi$ is a scalar field. $\boldsymbol{H}_{\mathrm{c}}$ is the magnetic field strength in the conducting domain. The cohomology source field $\boldsymbol{H}_I$ is used to impose the total current to the HTS tape [12]. The basis of $\boldsymbol{H}_I$, consisting of the red edges, is shown in Fig. 1. Moreover, $\boldsymbol{H}_I$ and $\boldsymbol{H}_{\mathrm{c}}$ are interpolated with Whitney-1 forms [13], i.e. with edge-elements.

### B. Material Models

As shown in, Fig. 1, the modeling domain consists of different materials. The models for them at 77 K temperature are detailed next. Copper, silver and Hastelloy are assumed to have constant resistivities: $\rho_{\mathrm{Cu}} = 2.9 \cdot 10^{-9}\,\Omega\mathrm{m}$, $\rho_{\mathrm{Ag}} = 2.8 \cdot 10^{-9}\,\Omega\mathrm{m}$ and $\rho_{\mathrm{Hast}} = 10^{-6}\,\Omega\mathrm{m}$. Moreover, $\mu$ is assumed to be equal to the permeability of free space $\mu_0$ everywhere.

The nonlinear resistivity of the superconducting material is modeled using the power law

$$\rho = \frac{E_{\mathrm{c}}}{J_{\mathrm{c}}} \left( \frac{|\boldsymbol{J}|}{J_{\mathrm{c}}} \right)^{n-1}, \tag{3}$$

where $|\cdot|$ is the Euclidean norm, $n = 30.5$, critical electric field strength $E_{\mathrm{c}} = 10^{-4}$ V/m and $J_{\mathrm{c}}$ is the critical electric current density. The critical current density is modeled here with the two different models: the Bean model and the Kim model [11]. In the Bean model, $J_{\mathrm{c}}$ equals to a constant $J_{\mathrm{c0}}$ $(= 2.85 \cdot 10^{10}$ A/m) while in the Kim model, $J_{\mathrm{c}}$ is an anisotropic function of $\boldsymbol{H}$:

$$J_{\mathrm{c}} = J_{\mathrm{c0}} \left( 1 + \frac{\mu_0}{B_0} |\boldsymbol{H}_k| \right)^{\beta}, \tag{4}$$

where $\boldsymbol{H}_k = [kH_x,\ H_y,\ 0]^{\mathrm{T}}$, $k = 0.29515$, $B_0 = 42.65$ mT and $\beta = -0.7$ as reported in [11].

### C. Models in Time

The two different models in time under comparison in this work are the TTM and the MHM. In the TTM, the simulation problem is solved at discretized instants of time $t_{i+1} = t_i + \Delta t$, where $\Delta t$ is the length of the time-step. In this work, constant $\Delta t$ was used. Hence, the time derivative of a field $\boldsymbol{F}$ can be approximated using for example the Backward Euler Method as

$$\partial_t \boldsymbol{F}(\boldsymbol{x}, t_{i+1}) = \frac{\boldsymbol{F}(\boldsymbol{x}, t_{i+1}) - \boldsymbol{F}(\boldsymbol{x}, t_i)}{\Delta t}. \tag{5}$$

In the multiharmonic method, a truncated Fourier series is used as the global basis in time to approximate a time-varying field $\boldsymbol{F}$ as

$$\boldsymbol{F}(\boldsymbol{x}, t) = \boldsymbol{F}_0(\boldsymbol{x}) + \sum_{k=1}^{N} \boldsymbol{F}_{sk}(\boldsymbol{x}) \sin(k\omega t) + \boldsymbol{F}_{ck}(\boldsymbol{x}) \cos(k\omega t). \tag{6}$$

The coefficients $\boldsymbol{F}_0$, $\boldsymbol{F}_{sk}$ and $\boldsymbol{F}_{ck}$ are spatially unknown vector fields to be solved with FEM. The total number of the fields in the full approximation equals to $2N + 1$. The angular frequency is $\omega = 2\pi f_0$, where $f_0$ is the fundamental frequency. Different harmonics are defined by the integer $k = 1, \ldots, N$. Moreover, a harmonic is odd when $k$ is an odd number and even when $k$ is an even number. In the simulations carried out in this work, the source current will be driven at the fundamental frequency, i.e., at odd frequency. Consequently, using the material models defined in Section II-B, the multiharmonic solution consists only of the odd harmonics [9]. Consequently, in this work, the multiharmonic field approximations are of the form

$$\boldsymbol{F}(\boldsymbol{x}, t) = \sum_{k=1,3,5,\ldots}^{N} \boldsymbol{F}_{sk}(\boldsymbol{x}) \sin(k\omega t) + \boldsymbol{F}_{ck}(\boldsymbol{x}) \cos(k\omega t) \tag{7}$$

Therefore, the total number of unknown fields is reduced to $N + 1$, where $N$ is odd.

Other global bases for the time domain could be used. For simulation tasks, where the total current is ramped up linearly, the Chebyshev polynomials having a linear component in the basis functions can be a better choice than the Fourier basis functions.

### D. Newton Method for Solving the Nonlinear Problem

In this work, the electric field $\boldsymbol{E}$, depending nonlinearly on $\boldsymbol{J}$ and $\boldsymbol{H}$ is approximated using the Taylor series at the known

fields $(\boldsymbol{J}_0, \boldsymbol{H}_0)$ as

$$\boldsymbol{E} \approx \boldsymbol{E}(\boldsymbol{J}_0, \boldsymbol{H}_0) + \frac{\partial \boldsymbol{E}}{\partial \boldsymbol{J}}(\boldsymbol{J} - \boldsymbol{J}_0) + \frac{\partial \boldsymbol{E}}{\partial \boldsymbol{H}}(\boldsymbol{H} - \boldsymbol{H}_0), \quad (8)$$

where the current field value of $\boldsymbol{E}$ and the derivatives of it with respect to $\boldsymbol{J}$ and $\boldsymbol{H}$ are evaluated at the known field values $(\boldsymbol{J}_0, \boldsymbol{H}_0)$ solved at the previous iteration.

This linearisation (8) is substituted into the strong formulation (1). From there on, standard FEM is applied to solve the equation iteratively until the desired tolerance is met. In the multiharmonic method, the nonlinear expression $\boldsymbol{E}$ and its derivatives are transformed into frequency domain using the discrete Fourier transform. Consequently, the assembled matrix equation of the weak formulation consists of the spatial degrees of freedom (DoF) for all the fields in the series. In the MHM, the spatial solution as a function of time is obtained by solving the nonlinear problem iteratively only once. In the TTM, the nonlinear problem is solved at each time-step.

## III. Results and Discussion

The modeling domain geometry and the corresponding mesh were created using Gmsh [14], which was used for solving the cohomology basis for setting the tape's total current. The MHM and the TTM solvers were implemented using the open-source FEM C++ library Sparselizard [15].

In the simulations, the main focus was in comparing the steady-state AC losses obtained with the MHM and the TTM.

The two different models for $J_c$, detailed in Section II-B, are compared: the Bean and Kim models. In all the simulations, total current of

$$I(t) = 0.8 I_{c0} \sin(\omega t) \quad (9)$$

was enforced to flow through the tape-cross section, where $I_{c0} = 114$ A and $\omega = 2\pi 50$ rad/s. The resulting AC losses $P$ over the cross-section of the tape, were computed as a function of time as

$$P(t) = \int_{\Omega_{\text{tape}}} \boldsymbol{E}(t) \cdot \boldsymbol{J}(t) \, \mathrm{d}\Omega, \quad (10)$$

where $\Omega_{\text{tape}}$ is the area of the tape cross-section.

The reference solutions for the comparisons between the TTM and the MHM were obtained using the TTM, with the two $J_c$ models. Only one period of the excitation was computed and for the TTM, the steady-state AC loss over the cycle converged with $\sim$900 time-steps. Note that the TTM solution was assumed to be in the steady-state after the first half of the cycle. Furthermore, the reference solutions obtained with the TTM were compared against the predictions given by the alternative simulation approach using the MHM. The first comparison was based on the relative difference computed as

$$\frac{|L_{\text{TTM}} - L_{\text{MHM}}|}{L_{\text{TTM}}}, \quad (11)$$

where $L_{\text{TTM}}$ is the steady-state loss over the cycle computed with the TTM and $L_{\text{MHM}}$ is the loss over cycle computed with the MHM.

Fig. 2 shows the relative difference between the steady-state losses over the cycle predicted with MHM in comparison to the losses given by the TTM. Based on the results, the accuracy

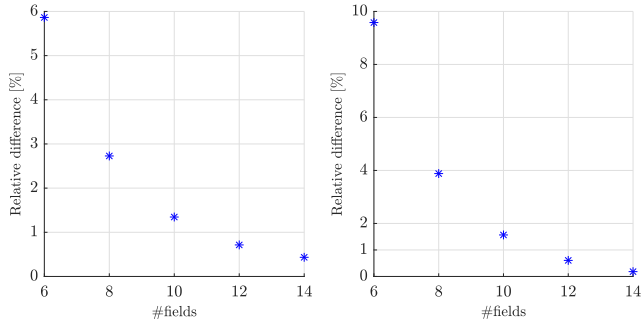


Fig. 2. Relative difference between the MHM and the TTM in the steady-state AC losses as a function of number of fields in the Fourier series approximation. Left: Bean model. Right: Kim model.

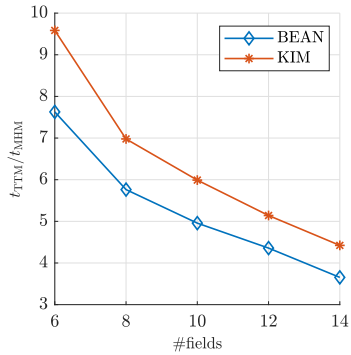


Fig. 3. Comparing simulation time as a function of the number fields in the Fourier series.

of the multiharmonic method increases with increasing number of fields in the Fourier series used to approximate the electromagnetic fields. Using 10 fields (five harmonics), the relative difference to the TTM is $\sim$1.5% with the both Bean and Kim models. Using 14 fields (7 harmonics), the relative differences of 0.4% (Bean) and 0.2% (Kim) were obtained.

We also compared the simulation time of MHM ($t_{\text{MHM}}$) as a function of the number of fields to the simulation time required to solve the problem with the TTM ($t_{\text{TTM}}$). The comparison is shown in Fig. 3 as the fraction $t_{\text{MHM}}/t_{\text{TTM}}$. With 10 unknown fields, MHM was 5-6 times faster with the relative difference of $\sim$1.5% in both cases. This comparison is only indicative since the TTM and the MHM are very different methods by nature. However, it can be concluded that the less fields can be used, the faster the MHM is in comparison to the TTM.

To get a more detailed comparison, Fig. 4 compares the AC loss as a function of time for the Bean and Kim models in case of 14 fields. In the results obtained with the TTM, a transient phase can be seen in the first half of the excitation period. For both the Bean and Kim models, the MHM agrees well with the TTM given results. Hence, we can conclude that the MHM based approach is able to predict succesfully the AC losses in the given simulation task.

A point-wise comparison of the norm of the magnetic flux density $|\boldsymbol{B}|$ obtained with the MHM and the TTM is shown in Fig. 5, where $|\boldsymbol{B}|$ is interpolated in the center of the HTS layer along the width of the tape. The $|\boldsymbol{B}|$-profiles are shown at $3/4\,T$, where $T$ is the duration of the period. Hence, the total current is at its minimum ($-0.8 I_{c0}$). The comparison is shown for both the

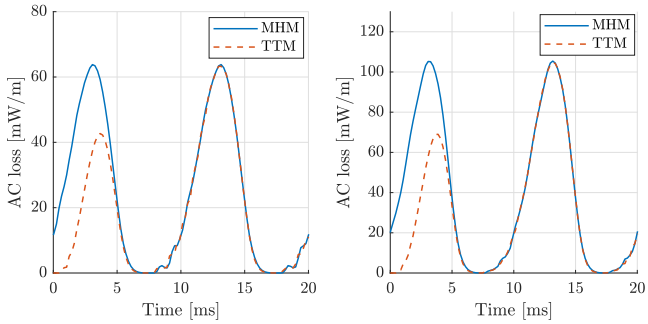


Fig. 4. Comparison of the AC losses as a function of time. Left: Bean model. Right: Kim model.

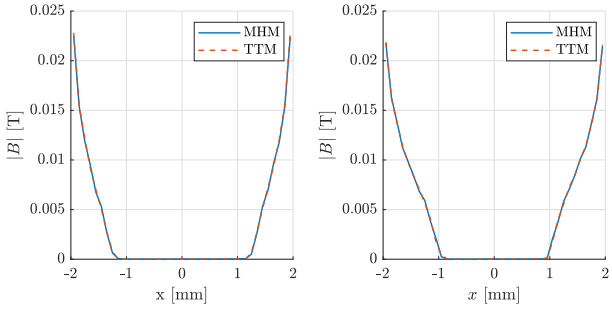


Fig. 5. Comparing the norm of the magnetic flux density in the center of the HTS layer along the width of the tape. Left: Bean model. Right: Kim model.

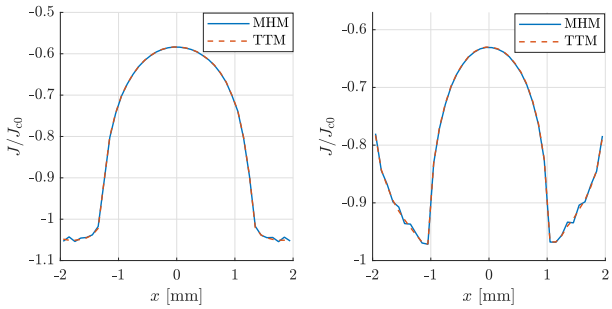


Fig. 6. Comparing the out-of-plane component of $\boldsymbol{J}$, normalized with $J_{c0}$, in the center of the HTS layer along the width of the tape. Left: Bean model. Right: Kim model.

Bean and Kim models. The results show that the MHM is able to predict the magnetic flux density profile in the given simulation task using the Bean and Kim models.

Fig. 6 compares the current density profile in the HTS tape predicted with the MHM and the TTM using the Bean and the Kim models. For the comparison, the out-of-plane component of the current density, normed with $J_{c0}$, was interpolated in the center of the HTS layer along the width of the tape. The results show an agreement between the MHM and the TTM for the both $J_c$ models. However, $\boldsymbol{J}$ does not seem to be as smooth in the saturated region as in the case of the TTM. This can be related to the truncated Fourier series and/or different requirements on the mesh density or interpolation order in comparison to the TTM.

As a final comparison, Fig. 7 shows average loss in the superconducting tape as a function of the excitation frequency. Results were computed using both the MHM and TTM with the Bean and

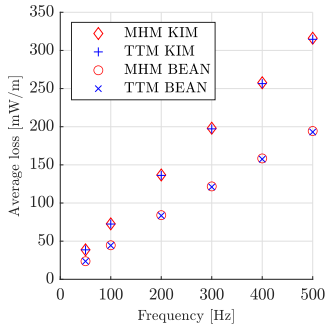


Fig. 7. Average loss as a function of source current frequency simulated using the MHM and the TTM with Bean and Kim models.

Kim models. Good agreement was observed between the MHM and TTM. Furthermore, the average losses increased linearly with increasing frequency, and higher losses were obtained with the Kim model than the Bean model.

## IV. Conclusion

In this paper, the multiharmonic method using global basis functions in the time domain was demonstrated by predicting computationally the eddy current losses and field quantities in REBCO HTS tape cross-section using the finite element method. The approach was succesfully validated in a test simulation case against the simulation results given by the conventional time-transient method. In the comparison, the $H-\varphi$ formulation was used for both approaches with two different $J_c$ models: Bean and Kim, where in the Kim model the anisotropic dependency of the magnetic field on the resistivity of the superconducting material was taken into account.

In the test case, total electric current at 50 Hz frequency was applied through the HTS tape cross-section. The main interest in the comparisons was how accurately the MHM approach was able to predict the steady-state AC losses over one period of excitation. As expected, the accuracy of the MHM based approach increased when the number of fields in the Fourier series was increased. With 14 fields, the relative difference to AC losses per cycle obtained with the TTM was 0.2% with Kim model and 0.4% with Bean model.

Even though the degrees of freedom in the FEM problem to be solved for 14 fields was 14 times the DoFs needed for the TTM (5001), the multiharmonic method was still faster in the simulation test case investigated in this work. With 10 fields, the MHM was 5-6 times faster than the TTM with only $\sim$1.5% relative difference in the steady-state AC losses per cycle. An additional succesful comparison was also carried out where MHM and TTM were compared by simulating average losses as a function of applied current density. The results showed that the average losses increased linearly with the increasing frequency.

As the future work, the efficiency of the MHM approach, in comparison to the TTM, should be tested by simulating a stack of tapes in 2-D and 3-D modelling domains. In addition, other global bases for the time domain could be investigated such as the Chebyshev polynomials.

## REFERENCES


[1] D. Uglietti, "A review of commercial high temperature superconducting materials for large magnets: From wires and tapes to cables and conductors," *Supercond. Sci. Technol.*, vol. 32, no. 5, Apr. 2019, Art. no. 053001. [Online]. Available: https://doi.org/10.1088/1361-6668/ab06a2

[2] L. Rossi and C. Senatore, "HTS accelerator magnet and conductor development in Europe," *Instruments*, vol. 5, no. 1, 2021, Art. no. 8. [Online]. Available: https://www.mdpi.com/2410-390X/5/1/8

[3] W. A. Soomro, Y. Guo, H. Y. Lu, and J. X. Jin, "Advancements and impediments in applications of high-temperature superconducting material," in *Proc. IEEE Int. Conf. Appl. Supercond. Electromagn. Devices*, 2020, pp. 1–4.

[4] A. Molodyk et al., "Development and large volume production of extremely high current density YBa2Cu3o7 superconducting wires for fusion," *Sci. Rep.*, vol. 11, no. 1, pp. 1–11, 2021.

[5] W. Goldacker, F. Grilli, E. Pardo, A. Kario, S. I. Schlachter, and M. Vojenčiak, "Roebel cables from REBCO coated conductors: A one-century-old concept for the superconductivity of the future," *Supercond. Sci. Technol.*, vol. 27, no. 9, Aug. 2014, Art. no. 093001.

[6] Q. Wu et al., "Electromagnetic and mechanical properties of CORC cable due to screening current," *Supercond. Sci. Technol.*, vol. 35, no. 7, May 2022, Art. no. 075005. [Online]. Available: https://dx.doi.org/10.1088/1361-6668/ac6c5b

[7] S. Kar et al., "Next-generation highly flexible round REBCO STAR wires with over 580 a $mm^2$ at 4.2 K, 20 T for future compact magnets," *Supercond. Sci. Technol.*, vol. 32, no. 10, Aug. 2019, Art. no. 10LT01. [Online]. Available: https://dx.doi.org/10.1088/1361-6668/ab3904

[8] D. M. Copeland and U. Langer, "Domain decomposition solvers for nonlinear multiharmonic finite element equations," *J. Numer. Math.*, vol. 18, no. 3, pp. 157–175, 2010.

[9] J. Gyselinck, P. Dular, C. Geuzaine, and W. Legros, "Harmonic-balance finite-element modeling of electromagnetic devices: A novel approach," *IEEE Trans. Magn.*, vol. 38, no. 2, pp. 521–524, Mar. 2002.

[10] V. Lahtinen, A. Stenvall, F. Sirois, and M. Pellikka, "A finite element simulation tool for predicting hysteresis losses in superconductors using an H-oriented formulation with cohomology basis functions," *J. Supercond. Novel Magnetism*, vol. 28, no. 8, pp. 2345–2354, 2015.

[11] B. C. Robert, M. U. Fareed, and H. S. Ruiz, "How to choose the superconducting material law for the modelling of 2G-HTS coils," *Materials*, vol. 12, no. 17, 2019, Art. no. 2679. [Online]. Available: https://www.mdpi.com/1996-1944/12/17/2679

[12] M. Pellikka, S. Suuriniemi, L. Kettunen, and C. Geuzaine, "Homology and cohomology computation in finite element modeling," *SIAM J. Sci. Comput.*, vol. 35, no. 5, pp. B1195–B1214, 2013.

[13] A. Bossavit, "Whitney forms: A class of finite elements for three-dimensional computations in electromagnetism," *IEE Proc. A. (Phys. Sci., Meas. Instrum., Manage. Educ., Rev.)*, vol. 135, no. 8, pp. 493–500, 1988.

[14] C. Geuzaine and J.-F. Remacle, "GMSH: A 3-D finite element mesh generator with built-in pre- and post-processing facilities," *Int. J. Numer. Methods Eng.*, vol. 79, no. 11, pp. 1309–1331, 2009.

[15] A. Halbach, "Sparselizard - the user friendly finite element C library," 2017. [Online]. Available: https://www.sparselizard.org/